buildings

MDPI

Article

Shaking Table Test of a Base-Isolated Frame Structure under Near-Fault Ground Motions

Qing Lyu [1], Baijie Zhu [2,3], Wensheng Lu [4], Bo Fu [5,*], Liangkun Liu [6], Wei Qian [1], Ming Zhou [1] and Zhenya Zhang [1]

1 School of Civil and Transportation Engineering, Ningbo University of Technology, Ningbo 315211, China
2 Key Laboratory of Earthquake Engineering and Engineering Vibration, Institute of Engineering Mechanics, China Earthquake Administration, Harbin 150080, China
3 Key Laboratory of Earthquake Disaster Mitigation, Ministry of Emergency Management, Harbin 150080, China
4 State Key Laboratory of Disaster Reduction in Civil Engineering, Tongji University, Shanghai 200092, China
5 School of Civil Engineering, Chang'an University, Xi'an 710061, China
6 School of Environment and Civil Engineering, Dongguan University of Technology, Dongguan 523808, China
* Correspondence: 90_bofu@chd.edu.cn

Abstract: A five-story moment frame structural model with a base isolation system was tested on a shaking table. The isolation system comprised both linear natural rubber bearing (LNR) and nonlinear viscous dampers (NLVDs). Seven ground motions were employed: including three far-fault (FF) and four near-fault (NF) earthquake ground motions. The performance of the isolation system was evaluated by measuring the displacement and base shear of the isolation bearings. Furthermore, the axial force and displacement of the NLVDs were measured. The evolution of the fundamental dynamic frequency of the frame during the test was also determined. During strong earthquakes, NF ground motions caused larger story drifts and floor accelerations of the superstructure than FF ground motions. The displacement and base shear of the isolation base was very large when the isolated structure was subjected to Kobe_TAK000 and ChiChi_TCU102/278 pulse-like NF ground motions. Furthermore, the LNR s experienced tension and uplift when the PGA of input earthquake ground motions was larger than 0.80 g. Although the NLVDs performed very well in combination with the LNRs, the severe responses of the isolation bearings were caused by NF ground motion with a pulse period T_p neighboring the fundamental period of the isolated structure.

Keywords: base isolation; near-fault (NF) ground motions; linear natural rubber bearing (LNR); nonlinear viscous damper (NLVD); shaking table test; seismic responses

Citation: Lyu, Q.; Zhu, B.; Lu, W.; Fu, B.; Liu, L.; Qian, W.; Zhou, M.; Zhang, Z. Shaking Table Test of a Base-Isolated Frame Structure under Near-Fault Ground Motions. *Buildings* **2022**, *12*, 2258. https://doi.org/10.3390/buildings12122258

Academic Editor: Weixin Ren

Received: 7 November 2022
Accepted: 15 December 2022
Published: 18 December 2022

1. Introduction

Base isolation is an effective passive control technique employed to protect buildings from earthquake-related damage. However, near-fault (NF) earthquakes with high-energy pulses cause more serious damage to isolated structures than far-fault (FF) earthquakes. NF earthquakes usually refer to an earthquake that is no more than 20 km away from the fault. Large displacement demand of isolation bearings will be caused by NF earthquakes with long-period pulses because a large amount of energy was put into the base isolation structures. The base isolation structure yield fewer cycles of high inelastic deformations to dissipate the energy, which may lead to severe damage or failure of base isolation systems [1,2]. Thus, numerous analytical studies have been performed on the seismic performance of base-isolated structures subjected to NF ground motions. Elastomeric bearings can effectively reduce the seismic response of the superstructure under FF ground motions containing medium-high frequency by affording large energy content. However, the seismic response of the base isolation structure will be amplified under NF ground motions in comparison with that of the corresponding fixed-base structure [3]. Jangid and Kelly [4] analyzed the damping effect on the seismic performance of isolation systems under NF ground motions, and they determined that there exists optimum damping of the isolation system to minimize acceleration responses of superstructures. Jangid [5] investigated seismic responses of buildings isolated by lead-rubber bearings (LRB) under NF ground motions. Parameters including isolation period, bearing yield strength, and superstructure flexibility were employed to analyze the seismic performance of the superstructure and isolation system. The results indicate that for the bearing with low yield strength, significant displacement will be caused by NF ground motions. Providakis [6] conducted a nonlinear statistical analysis and showed that base-isolated buildings could experience extreme nonlinear behavior under NF ground motions. Mazza and Vulcano [7] determined that supplemental viscous damping at the base effectively reduces the isolator displacement, but seismic responses of the superstructure could not be guaranteed in all cases, especially for relatively short pulse periods. The seismic performance of base-isolated buildings under bi-directional NF and FF ground motions was also investigated by Bhagat and Wijeyewickrema [8], and the results showed that NF ground motions afford larger superstructure and isolation system seismic demands than FF ground motions. Fling-step and forward-directivity characteristics of NF ground motions have an important effect on the seismic response of the base-isolated building [9]. NF ground motions with fling-step characteristics induce larger seismic demands on the base-isolated superstructure than other ground motions.

Buckling or rupture of isolation bearings could be induced under NF ground motions containing long-period pulses [10]. Moreover, the frequency component of the ground motion transmitted to the superstructure can become critical when the pulse intensity induces plastic deformations of the superstructures [11]. Additionally, the structural response could be amplified due to the long duration of the pulse [12]. NF ground motions may afford one or more displacement pulses that will cause large isolator displacement. Large isolator displacements can be resolved using large isolators, but it is not economical. Viscous dampers or large lead plugs are usually used for deducing the displacement demands on isolators. However, these damping mechanisms are nonlinear and become less effective at large displacements.

Although supplemental damping can reduce displacements of isolation bearings, it increases the seismic response of the higher vibration modes of the superstructure. Too large a supplemental damping ratio could significantly increase the inter-story drifts and floor accelerations of the superstructures, consequently reducing the benefits of the base isolation system [4,13]. Moreover, if large supplemental damping is employed to control the displacement of isolation bearings at a rare earthquake level, the superstructure could not benefit from the base isolation system at a low-level earthquake because the isolation layer becomes heavily damped. Thus, the isolation system will not be effective when the building is subject to a moderate earthquake if a high damping value is employed for controlling large bearing displacement under rare earthquakes.

Numerous analytical studies have been recently conducted into the effect of the isolation parameters on the seismic of steel frames and the optimal design of isolation devices for steel frames [14–16]. The effect of the distribution of a viscous damper for steel frame structures was also investigated [17]. Some analytical studies investigated the use of a base-isolation system with passive control devices [13,18–20] to protect framed buildings under strong NF ground motions. The influence of characteristics of ground motion and parameters of the base isolation systems on the structural seismic responses was investigated [13,18–20]. To protect frame buildings from NF ground motions with large displacement, the challenge is the selection of mechanical properties that will improve the response of structures subjected to high-frequency spikes and low-frequency pulses. Base-isolation systems with passive control devices have afforded satisfactory performances for framed buildings under strong NF ground motions [18].

Previous studies paid special attention to the sensitivity of the structural response to the characteristics of both ground motions and base-isolation systems via numerical calculation. However, few studies have experimentally investigated the performance of isolation systems and superstructures subjected to NF ground motions. Herein, the seismic performance of a five-story frame structure isolated using LNRs under FF and NF ground motions is investigated via the shaking table test. Seven ground motions are simulated, including three FF ground motions and four NF ground motions, which were selected from the Imperial Valley, Kobe, and ChiChi earthquakes. Additionally, the base shear and vertical force of the isolation bearings, as well as the maximum deformation and residual displacement of the viscous dampers, are evaluated under a rare earthquake. The floor acceleration and inter-story drift ratio are also investigated.

2. Shaking Table Test Model

2.1. Structural Model

The shaking table test was conducted on scaled structural models that are similar to the prototype structure and subjected to the same ground motions. The model structures were constructed to have a length scale factor of S_l = 1/4, considering the dimensions and payload capacity of the shaking table. Since the model structures comprised the same steel materials as the prototype structure, their elastic modulus scale factor was S_E = 1.0. The acceleration scale was chosen to have a value of unity S_a = 1. Additional masses were used to obtain the total mass of the models $S_E/S_a \cdot S_l$ times lower than that of the full-scale prototype while scaling times by $S_l^{0.5} \cdot S_a^{-0.5}$; thus, the model experiences the same accelerations as the prototype structure and S_l times lower displacements. Table 1 presents the detailed scale factors used in the testing.

Table 1. Typical similitude factors of the model structure.

Quantity	Scaling Law	Similitude Factors	
Length	S_l	1/4	Controlling size
Displacement	S_l	1/4	
Elastic modulus	S_E	1.0	Controlling material
Stress	S_σ	1.0	
Strain	$S_\varepsilon = S_\sigma/S_E$	1.0	
Acceleration	S_a	1.0	Controlling acceleration
Mass density	$S_\rho = S_E/(S_a \cdot S_l)$	4.0	
Mass	$S_m = S_E \cdot S_l^2/S_a$	1/16	
Force	$S_F = S_E \cdot S_l^2$	1/16	
Damping	$S_C = S_E \cdot S_l^{1.5} \cdot S_a^{-0.5}$	1/8	
Time	$S_T = S_l^{0.5} \cdot S_a^{-0.5}$	0.5	
Frequency	$S_f = S_l^{-0.5} \cdot S_a^{0.5}$	2.0	
Velocity	$S_v = (S_l \cdot S_a)^{0.5}$	1/2	

According to the similarity theory, the required scaling factor for the material density is $S_\rho = 1/S_l$ = 4. However, the provided material density is the same as the prototype or S_ρ = 1 because the same material as the prototype was used to manufacture the model structure. Three concrete blocks with a weight of 8 kN were added on each floor to ensure the scale factor of the mass density satisfying similarity laws.

Figure 1 displays the scaled structural model. The model structure has five stories and a total height of 4.5 m from the base. The model structure has three bays in the longitudinal direction and one bay in the transverse direction; each bay is 1.2 m wide with total dimensions of 1.2 × 3.6 m^2. Concrete blocks were used to add mass to satisfy similitude laws, bringing the total weight, including the base, to 180 kN.

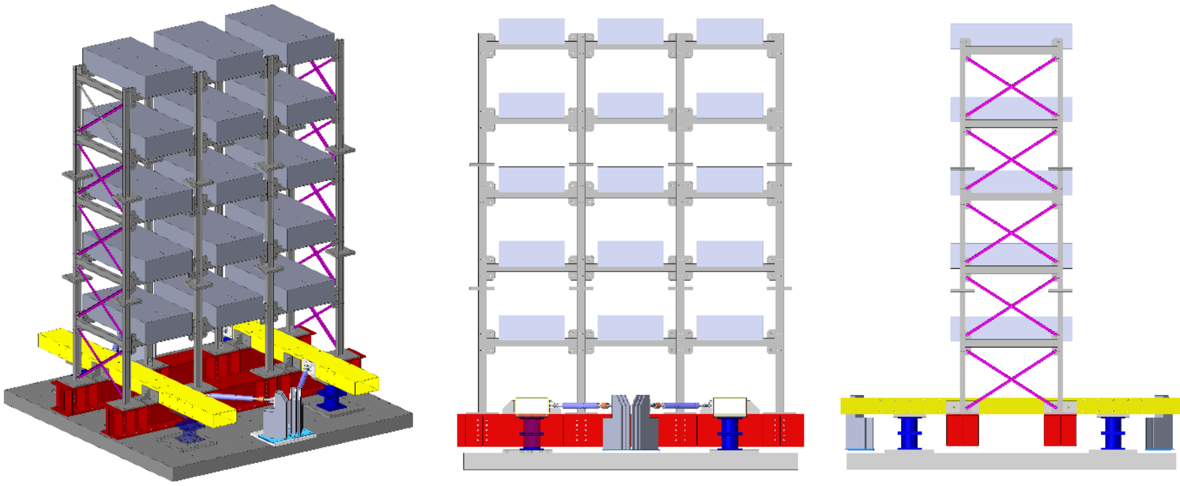

(**a**) (**b**) (**c**)

Figure 1. Model structure: (**a**) Steel structure model on the shaking table; (**b**) front and (**c**) side elevations of the steel structure model on the shaking table.

All columns and beams have a constant cross-section (I100 × 68 × 4.5 × 7.6). All bracings in the transverse direction are L40 × 4. All the beam–column joints are connected by bolts; thus, the model can be disassembled and transported using a truck. All beams and columns are rigidly connected by bolts at the flange and welded, ensuring the effective transformation of the bending moment and shear force. The superstructure is bolted to a basement with a grid of two I400 × 400 × 12 × 20 and two 400 × 200 × 10 tubes.

2.2. Base-Isolation Systems

Four low-damping rubber bearings (Figure 2a) were installed under the basement tubes to support the substructure. Four additional nonlinear viscous dampers (Figure 2c) were installed between the basement and the damper reaction support. Tables 2 and 3 list the mechanical properties of the rubber bearings and nonlinear viscous dampers, respectively.

Table 2. Mechanical properties of the LNRs.

Bearing Properties	Characterized Value in Model Domain
Characteristic Strength	7.53 kN
Post-yield Stiffness	182 kN/m
Initial Stiffness	2586 kN/m
Yield Displacement	2.0 mm
Effective Stiffness	200 kN/m
Designed displacement	80 mm
Maximum displacement	120 mm

Table 3. Mechanical properties of the NLVDs.

Damper Properties	Characterized Value in Model Domain
Damping coefficient C	30 kN s/m
α	0.5
Designed displacement	75 mm
Maximum displacement	112.5 mm
Maximum Force	30 kN
Maximum Velocity	1 m/s

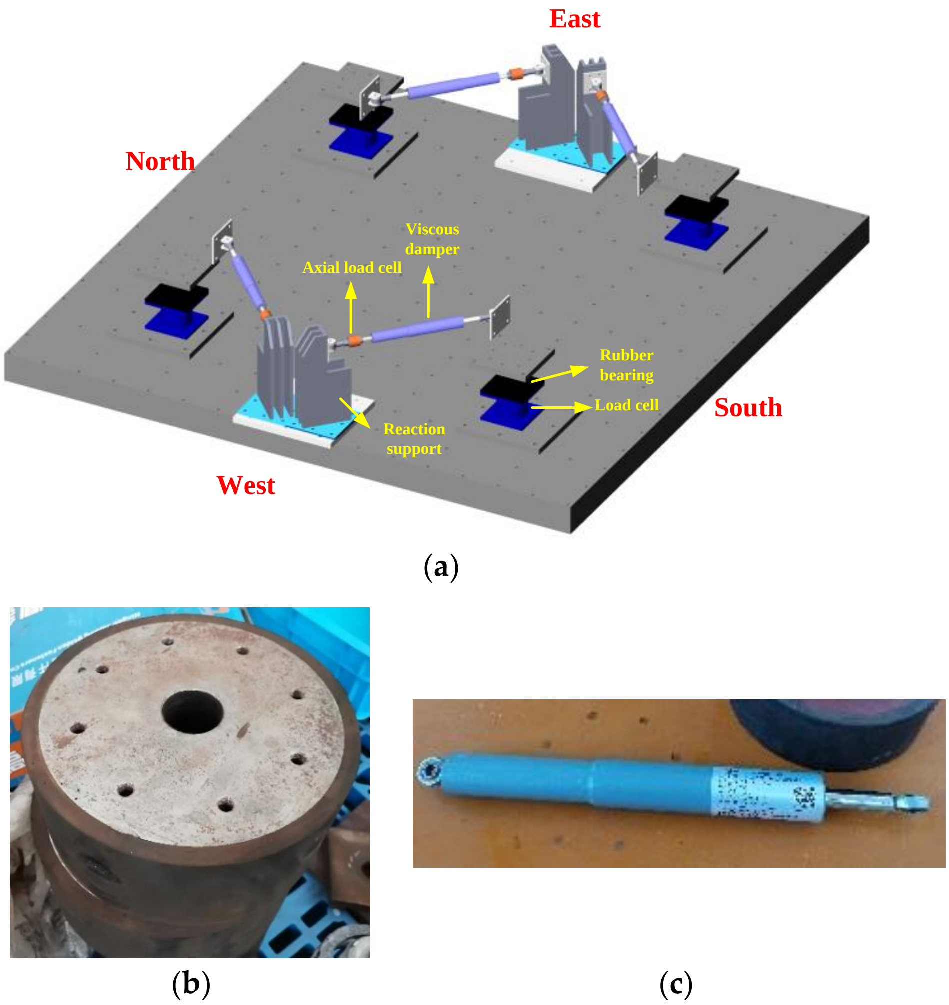

Figure 2. Base isolation system: (**a**) Layout of base isolation system; (**b**) LNR; (**c**) NLVD.

3. Test Program and Sensor Set-Up

3.1. Input Ground Motions

Table 4 shows the seven employed records for the shaking table test. The seven ground motions from the Kobe (1995), Chi-Chi (1999), and Imperial Valley (1979) earthquake events were chosen because they are all well-known in the field of earthquake engineering. The ground motion selected from Imperial Valley Earthquake at Delta station is a FF ground motion, and at Bonds Corner station is a NF ground motion. These two ground motions selected from the Imperial Valley Earthquake are referred to as Imp_F and Imp _N ground motions. The ground motion selected from the ChiChi Earthquake at TCU067 and TCU102 station is a NF ground motion, and at TCU045 station is a FF ground motion. The ground motion at TCU102 station had a pulse period of 9.632 s. These three ground motions selected from the ChiChi Earthquake are referred to as ChiChi_F, ChiChi_N, and ChiChi_NP ground motions, respectively. The ground motion selected from Kobe Earthquake at Shin Osaka is a FF ground motion, and at Takatori station is a pulse-like (T_p = 1.554 s) NF ground motion. These two ground motions selected from Kobe Earthquake are referred to as Kobe_F and Kobe_NP ground motions. Plots of the acceleration time histories for each motion scaled with a PGA of 1 m/s^2 are provided in Figure 3. The response spectrums of the seven ground motions are plotted in Figure 4.

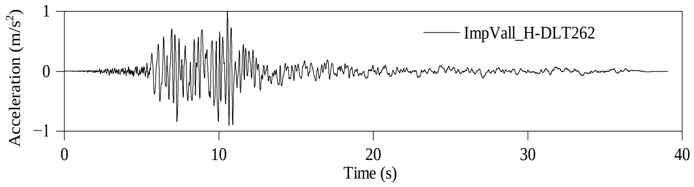

(**a**)

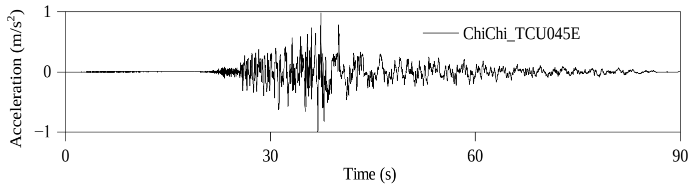

(**b**)

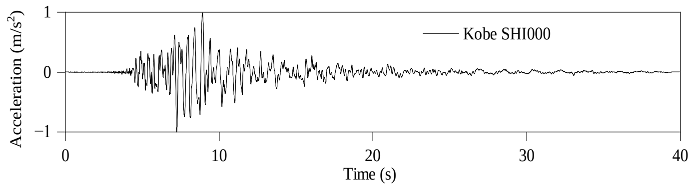

(**c**)

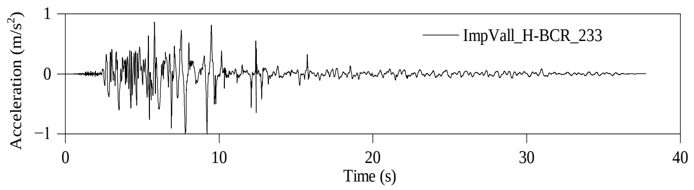

(**d**)

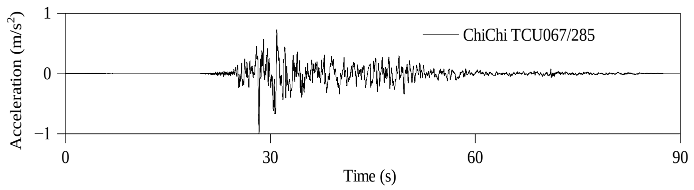

(**e**)

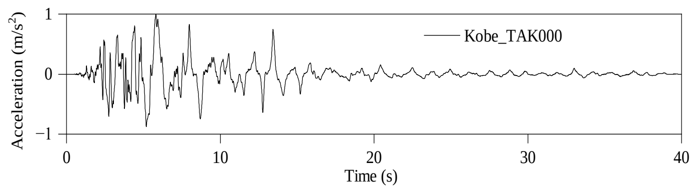

(**f**)

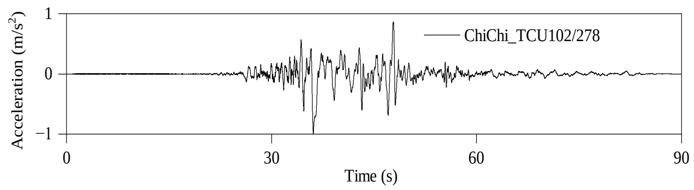

(**g**)

Figure 3. History of acceleration of the earthquake ground motions: (**a**) Imp_F; (**b**) Chihi_F; (**c**) Kobe_F; (**d**) Imp_N; (**e**) ChiChi_N; (**f**) Kobe_NP; (**g**) ChiChi_NP.

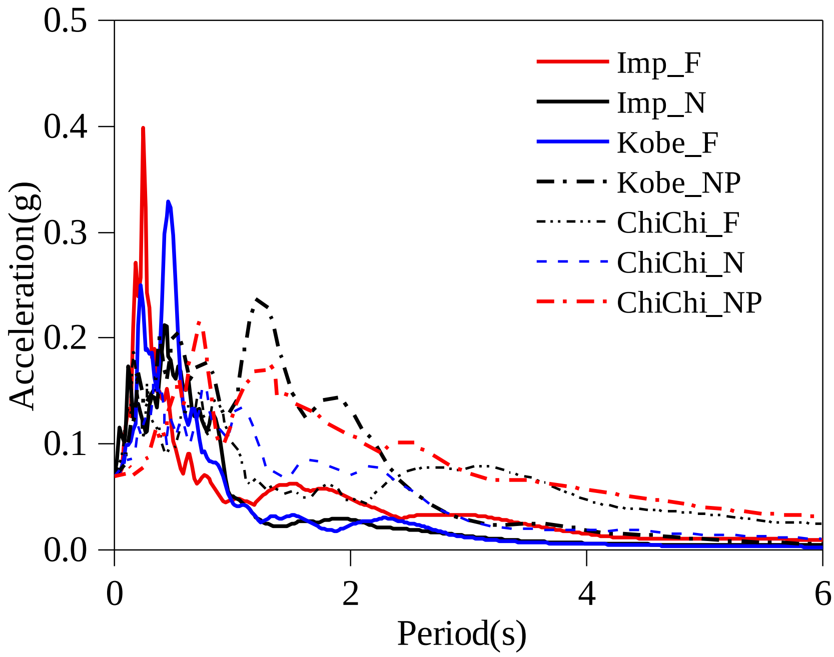

Figure 4. Acceleration response spectrum.

Table 4. Ground motions.

Earthquake	Station	Component Name	Component Name Abbreviation	Magnit-ude	PGA (g)	PGV (cm/s)	T_p (s)	R_{rup} (km)
Imperial Valley, 1979	Delta	ImpVall_H-DLT262	Imp_F	6.5	0.35	33	-	22.03
ChiChi, 1999	TCU045	ChiChi_TCU045E	ChiChi_F	7.6	0.51	39	-	26
Kobe, 1995	Shin Osaka	Kobe SHI000	Kobe_F	6.9	0.24	38	-	19.15
Imperial Valley, 1979	Bonds Corner	ImpVall_H-BCR233	Imp_N	6.5	0.76	44.3	-	2.66
ChiChi, 1999	TCU067	ChiChi_TCU067/285	ChiChi_N	7.6	0.56	91.8	-	0.62
Kobe, 1995	Takatori	Kobe_TAK000	Kobe_NP	6.9	0.28	120.67	1.554	1.47
ChiChi, 1999	TCU102	ChiChi_TCU102/278	ChiChi_NP	7.6	0.29	106.6	9.632	1.49

3.2. Test Program

The test program is listed in Table 5. White noise was used to identify the frequency and dynamic mode of the model structure. The PGA value of the white noise was 0.10 g. The PGAs of the earthquake ground motions were gradually increased from 0.1 g to 0.8 g.

3.3. Sensor Set-Up

Instruments were installed to record the actual shaking table motion, the isolation system response (isolation bearing horizontal deformations, horizontal and vertical forces, displacements, and axial forces of the viscous damper), and the superstructure response (absolute accelerations and displacements of each floor). The responses in the longitudinal direction were mainly measured.

Figure 5 displays the sensor arrangement. In the longitudinal direction, two accelerometers and two displacement sensors were installed at each of the five-floor levels and the basement. Two accelerometers and displacement transducers were installed at the northeast and southeast corners (Figure 5b) to record the torsional responses of the isolation system. In the transverse direction, accelerometers and displacement transducers were placed in the basement and each of the five stories. Six component (three force and three moment readings) load cells (Figure 5c) were installed under the isolation bearings to measure the shear force and axial force of the isolation bearings. Four dampers were arranged between the model structure basement and the damper reaction support. To measure the axial force of the damper, a uniaxial load cell was connected in series with the viscous damper.

Additionally, a laser displacement transducer was fixed on the outside of the damper barrel to measure the axial deformation of the viscous damper (Figure 5d).

Table 5. Test program.

Case Number	Case Name	Input	Input PGA
01	WN_01	White noise	0.10 g
02	Imp_F_0.10 g	Imp_F	0.10 g
03	ChiChi_F_0.10 g	ChiChi_F	0.10 g
04	Kobe_F_0.10 g	Kobe_F	0.10 g
05	Imp_N_0.10 g	Imp_N	0.10 g
06	ChiChi_N_0.10 g	ChiChi_N	0.10 g
07	Kobe_NP_0.10 g	Kobe_NP	0.10 g
08	ChiChi _NP_0.10 g	ChiChi _NP	0.10 g
09	WN 02	White noise	0.10 g
10	Imp_F_0.20 g	Imp_F	0.20 g
11	ChiChi_F_0.20 g	ChiChi_F	0.20 g
12	Kobe_F_0.20 g	Kobe_F	0.20 g
13	Imp_N_0.20 g	Imp_N	0.20 g
14	ChiChi_N_0.20 g	ChiChi_N	0.20 g
15	Kobe_NP_0.20 g	Kobe_NP	0.20 g
16	ChiChi _NP_0.20 g	ChiChi _NP	0.20 g
17	WN 03	White noise	0.10 g
18	Imp_F_0.30 g	Imp_F	0.30 g
19	ChiChi_F_0.30 g	ChiChi_F	0.30 g
20	Kobe_F_0.30 g	Kobe_F	0.30 g
21	Imp_N_0.30 g	Imp_N	0.30 g
22	ChiChi_N_0.30 g	ChiChi_N	0.30 g
23	Kobe_NP_0.30 g	Kobe_NP	0.30 g
24	ChiChi _NP_0.30 g	ChiChi _NP	0.30 g
25	WN 04	White noise	0.10 g
26	Imp_F_0.40 g	Imp_F	0.40 g
27	ChiChi_F_0.40 g	ChiChi_F	0.40 g
28	Kobe_F_0.40 g	Kobe_F	0.40 g
29	Imp_N_0.40 g	Imp_N	0.40 g
30	ChiChi_N_0.40 g	ChiChi_N	0.40 g
31	Kobe_NP_0.40 g	Kobe_NP	0.40 g
32	ChiChi _NP_0.40 g	ChiChi _NP	0.40 g
33	WN 05	White noise	0.10 g
34	Imp_F_0.60 g	Imp_F	0.60 g
35	ChiChi_F_0.60 g	ChiChi_F	0.60 g
36	Kobe_F_0.60 g	Kobe_F	0.60 g
37	Imp_N_0.60 g	Imp_N	0.60 g
38	ChiChi_N_0.60 g	ChiChi_N	0.60 g
39	Kobe_NP_0.60 g	Kobe_NP	0.60 g
40	ChiChi _NP_0.60 g	ChiChi _NP	0.60 g
41	WN 06	White noise	0.10 g
42	Imp_F_0.80 g	Imp_F	0.80 g
43	ChiChi_F_0.80 g	ChiChi_F	0.80 g
44	Kobe_F_0.80 g	Kobe_F	0.80 g
45	Imp_N_0.80 g	Imp_N	0.80 g
46	ChiChi_N_0.80 g	ChiChi_N	0.80 g
47	Kobe_NP_0.80 g	Kobe_NP	0.80 g
48	ChiChi _NP_0.80 g	ChiChi _NP	0.80 g
49	WN 07	White noise	0.10 g

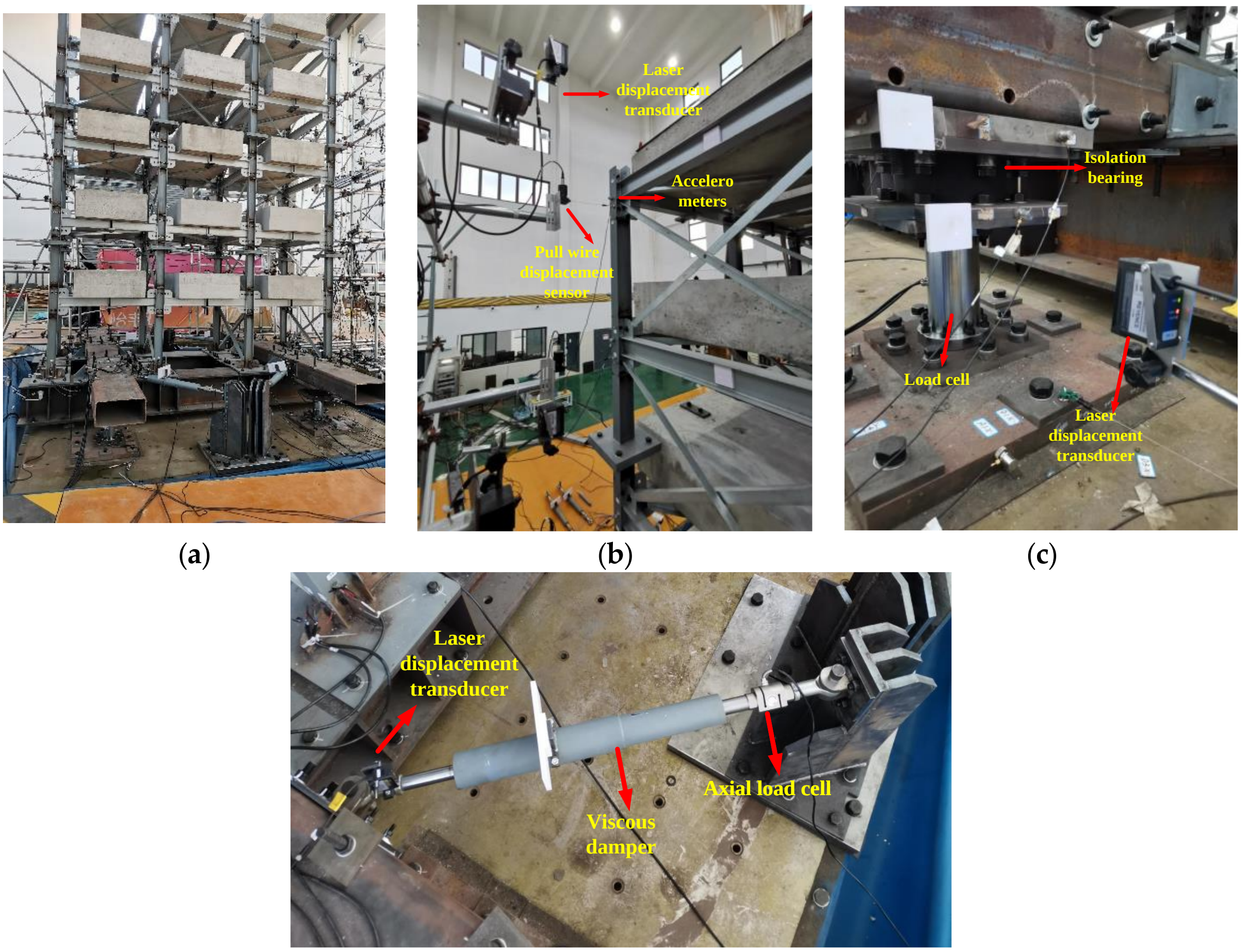

(**a**) (**b**) (**c**) (**d**)

Figure 5. Sensors of viscous dampers: (**a**) Test model structure; (**b**) Sensors of the superstructure; (**c**) Load cell—six components; (**d**) Sensors of NLVDs.

4. Shaking Table Test Results

4.1. Dynamic Modes

The white noise test results were used to identify the dynamic properties of the isolated structure in the longitudinal direction. The structure was subjected to a white noise excitation with frequencies ranging from 0 to 50 Hz and a PGA of 0.10 g. The transfer functions shown in Figure 6 were obtained as the ratio of the Fourier transform of the horizontal acceleration of each floor to the Fourier transform of the horizontal acceleration of the shaking table.

Based on the transfer function of the test acceleration results, the least square method was used to fit the transfer function curve. The frequency was obtained by searching the peak values of the real part of the transfer function curve, and the damping ratio was determined using the half-power broadband method. The modal frequencies corresponded to the local maxima of the amplitude of the transfer function. By measuring the amplitude of the transfer function at each floor, the mode shapes were determined from the ratios of the amplitudes for the frequency corresponding to one vibration mode. Additionally, the phase angles of the transfer function were determined to obtain the sign of the vibration mode shape. The damping ratios in each mode were calculated using the half-power bandwidth method around the transfer function peaks. The first five modes are shown in Figure 7, and the corresponding frequencies and damping ratios are listed in Table 6. It can be seen from the data in the table that the arrangement of NLVDs enhanced the damping ratio of the first three modes of the isolated structure.

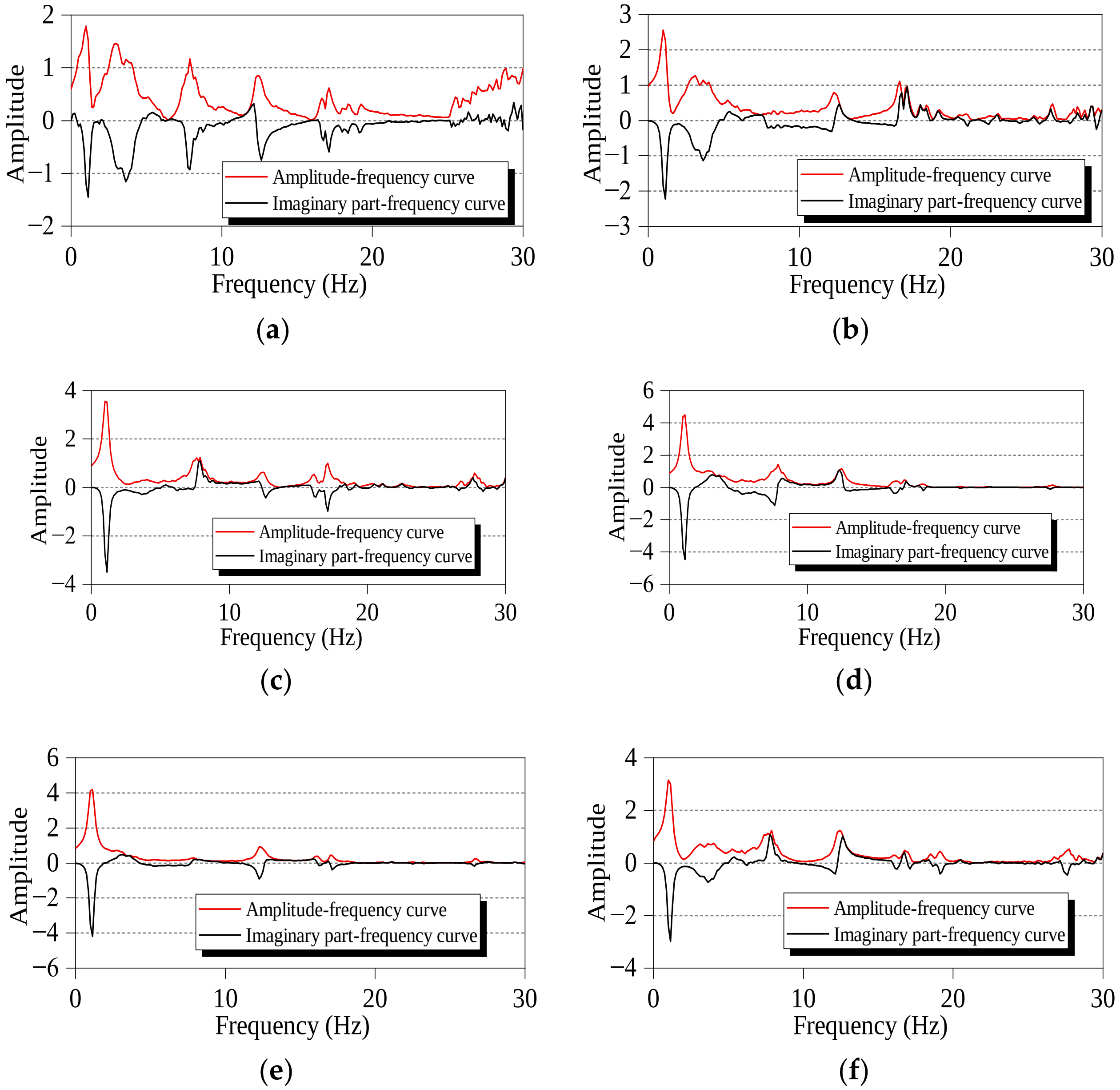

Figure 6. Amplitude and imaginary parts of the transfer function of the superstructure by WN05: (**a**) Basement; (**b**) First story; (**c**) Second story; (**d**) Third story; (**e**) Fourth story; (**f**) Fifth story.

Table 6. Frequencies and damping ratios of the first five modes.

Dynamic Property	**Mode**				
	1	**2**	**3**	**4**	**5**
Frequency (Hz)	1.1209	3.1053	7.8180	12.3631	16.7636
Damping ratio (%)	16.51	8.18	6.60	1.86	3.60

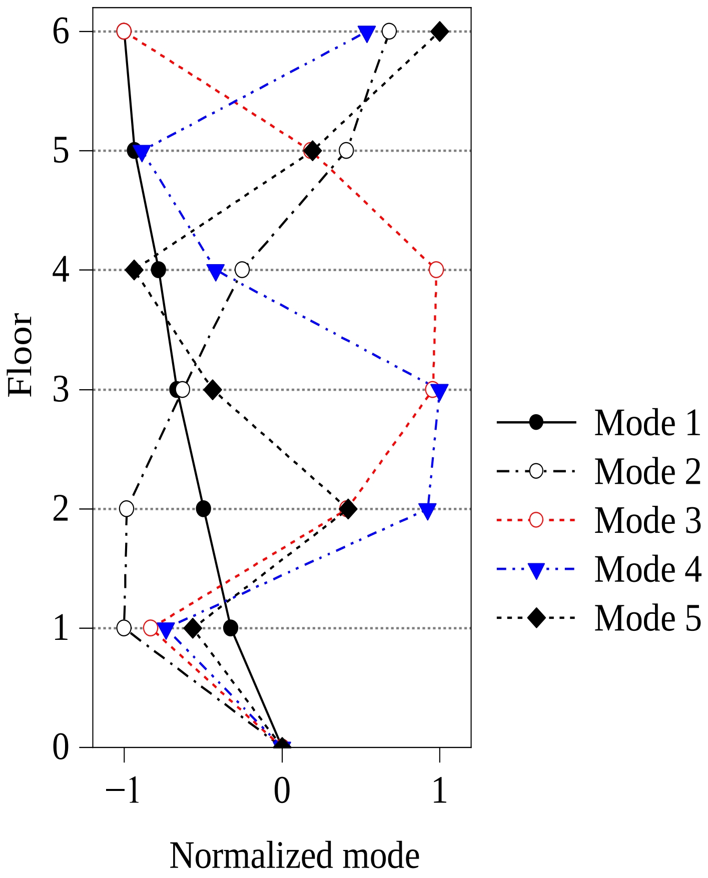

Figure 7. Mode shapes of the isolated structure.

4.2. Seismic Responses of the Frame Structures

Figure 8 displays the maximum inter-story drifts of the superstructure. It can be clearly seen from the figure that NF ground motions caused larger inter-story drifts than FF ground motions, especially when the input ground motion PGA exceeded 0.4 g. When the input PGA is 0.40 g, corresponding to the rare earthquake of intensity 8, the maximum inter-story drift of the superstructure is 0.72%, which is smaller than the specified value of 2% for the elastoplastic story drift in the current Chinese seismic code. When the input ground motion PGA was 0.60 g, the inter-story drifts caused by pulse-like NF ground motion were obviously larger than that caused by FF ground motion and NF ground motion without a pulse. The Kobe_NP ground motion caused the largest inter-story drift (1.32%) of the superstructure, followed by the ChiChi_NP pulse-like ground motion (0.959%). When the input ground motion PGA was 0.80 g, inter-story drifts of the superstructure caused by pulse-like NF ground motion were much larger than that caused by FF ground motion and NF ground motion without a pulse. The inter-story drift caused by ChiChi_NP ground motion was 1.79%. In contrast, the inter-story drift of the second and first floor of the superstructure caused by Kobe_NP ground motion was 2.79% and 3.15%, respectively. The measurement errors of the inter-story drifts of the third to the fifth floors were caused by the uplift of the LNRs. It can be drawn from the test results that the seismic responses of pulse-like NF ground motions are maximum, while those of the FF ground motions are minimum. The reason is that the principal frequency of the structure is closest to the main frequency content of the pulse-like NF ground motions and is furthest from that of the FF ground motions.

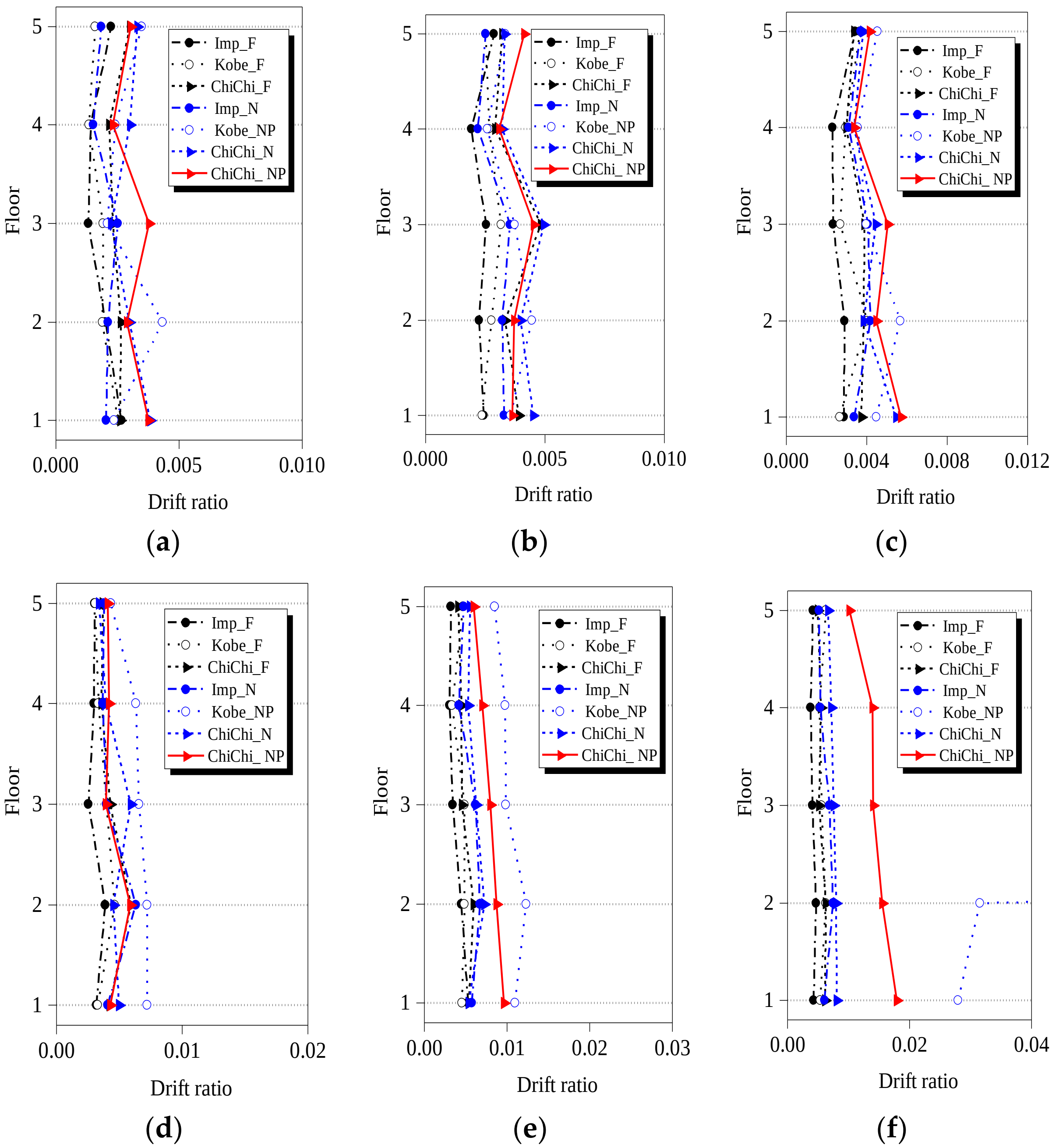

Figure 8. Maximum inter-story drifts of the superstructure: (**a**) PGA of 0.10 g; (**b**) PGA of 0.20 g; (**c**) PGA of 0.30 g; (**d**) PGA of 0.40 g; (**e**) PGA of 0.60 g; (**f**) PGA of 0.80 g.

Table 7 illustrates the amplification factors of the roof acceleration. The acceleration magnification was not obvious when the isolated structure was subjected to Imp_Fground motion, and the amplification factor was smaller than one when the input PGA was larger than 0.30 g. The amplification factor decreased gradually with the increased input PGA of the NF ground motions. The amplification factor increased when subjected to Kobe_NP and ChiChi_NP ground motions with a PGA of 0.80 g because of the impact of the substructure on the isolation bearing.

Table 7. Amplification factors of the roof acceleration.

Ground Motion	PGA (g)					
	0.10	**0.20**	**0.30**	**0.40**	**0.60**	**0.80**
Imp_F	1.09	1.02	0.87	0.92	0.91	0.87
Kobe_F	1.51	1.25	1.25	1.26	1.24	1.20
ChiChi_F	1.65	1.68	1.79	1.70	1.58	1.46
Imp_N	1.86	1.69	1.67	1.66	1.64	1.38
Kobe_N	1.46	1.45	1.15	1.10	1.05	1.57
ChiChi_N	1.80	1.72	1.49	1.36	1.19	1.15
ChiChi_NP	1.69	1.38	1.19	1.13	1.00	1.06

4.3. Performance Evaluation of the Isolation System under Earthquakes

The base shear shown in Figure 9 was calculated as the sum of the shear forces of the four isolation bearings divided by the total weight of the substructure. The presented base shear was normalized by the total weight, W, which is equal to 180 kN. The normalized base shear increased with the PGA of the input. When PGA was smaller than 0.6 g, the normalized base shear was smaller than one. The normalized base shear exceeded one when the isolation structure was subjected to Kobe-NP and ChiChi_NP ground motions, with a PGA of 0.8 g. The NF ground motions significantly affected the normalized base shear compared with FF ground motions. The Kobe_NP ground motion yields a considerably large normalized base shear for the isolation system.

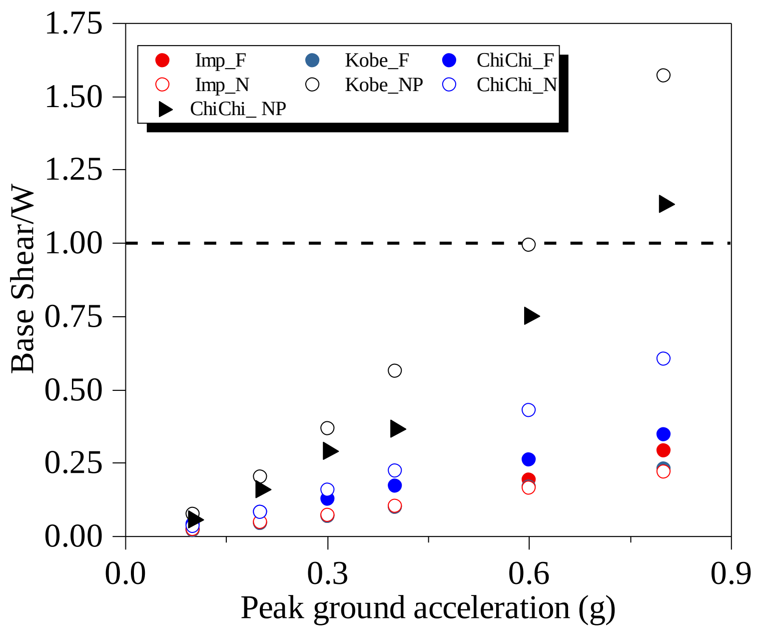

Figure 9. Base shear variation with the PGA of the ground motion inputs.

The overturning moment of the superstructure induced a substantial variation of the axial load on the north or south bearings. In a few cases, tension was afforded in the LNRs. Figures 10 and 11 present the histories of axial force on the bearings for the isolated moment frame structure subjected to the Kobe_NP_0.60 g and ChiChi_NP_0.60 g, respectively. The bottom graph in the figures displays the history of the total axial forces on all four bearings. When the ground motion PGA was 0.6 g, the total axial force on all four bearings slightly varied, indicating that there was little vertical acceleration on the model. In contrast, the total axial force in the two north and south bearings experienced large variations of the order of 100%. This considerable variation in the total axial force of four bearings indicates that a large overturning moment is present. As shown in Figure 10, the excitation PGA is 0.8 g, and the total axial force on all four bearings exhibited large variations due to the impact on the load cells after the uplift of the entire structure.

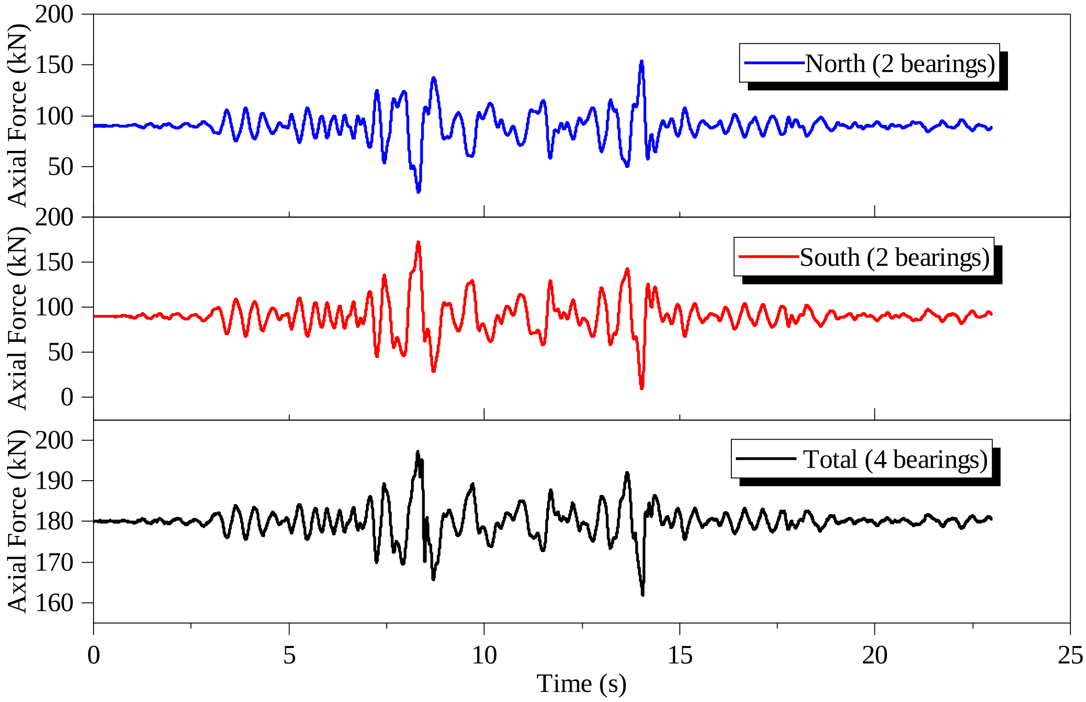

(**a**)

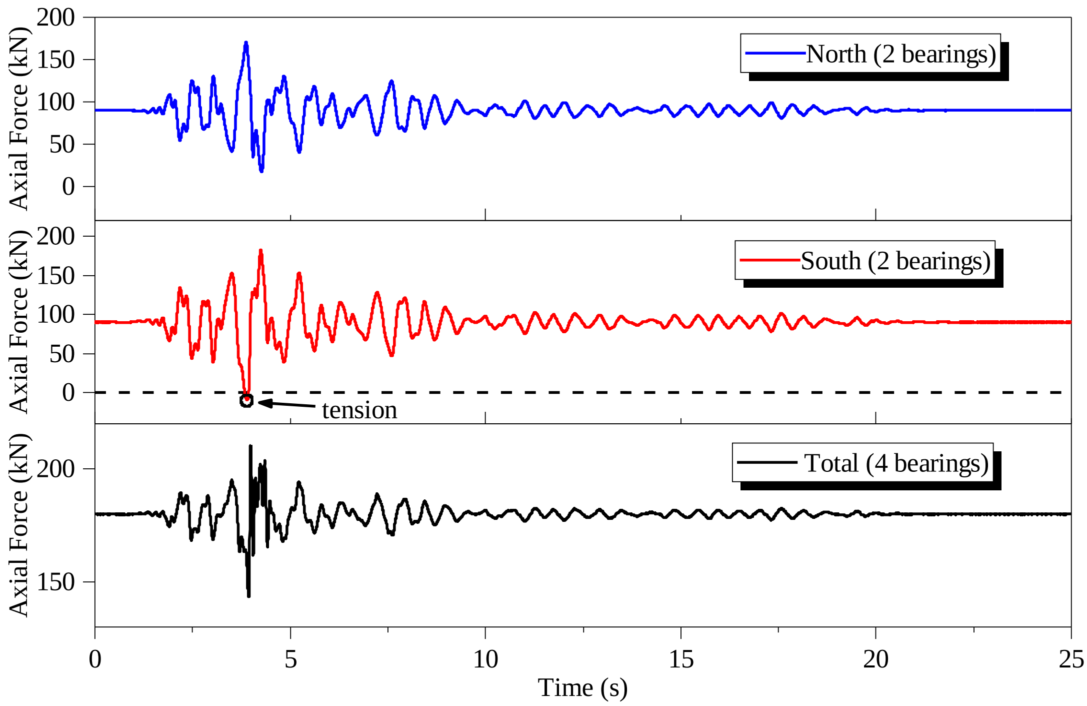

(**b**)

Figure 10. History of the record axial force of the LNRs subjected to: (**a**) ChiChi_NP_0.60 g; (**b**) Kobe_NP_0.60 g.

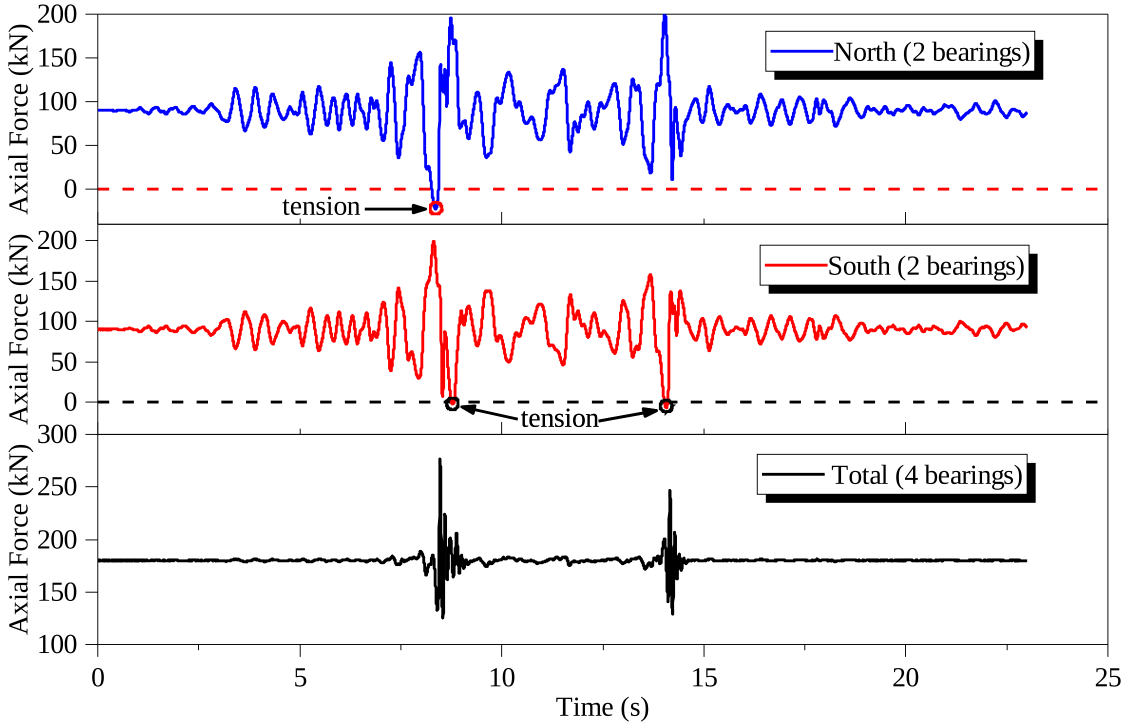

(**a**)

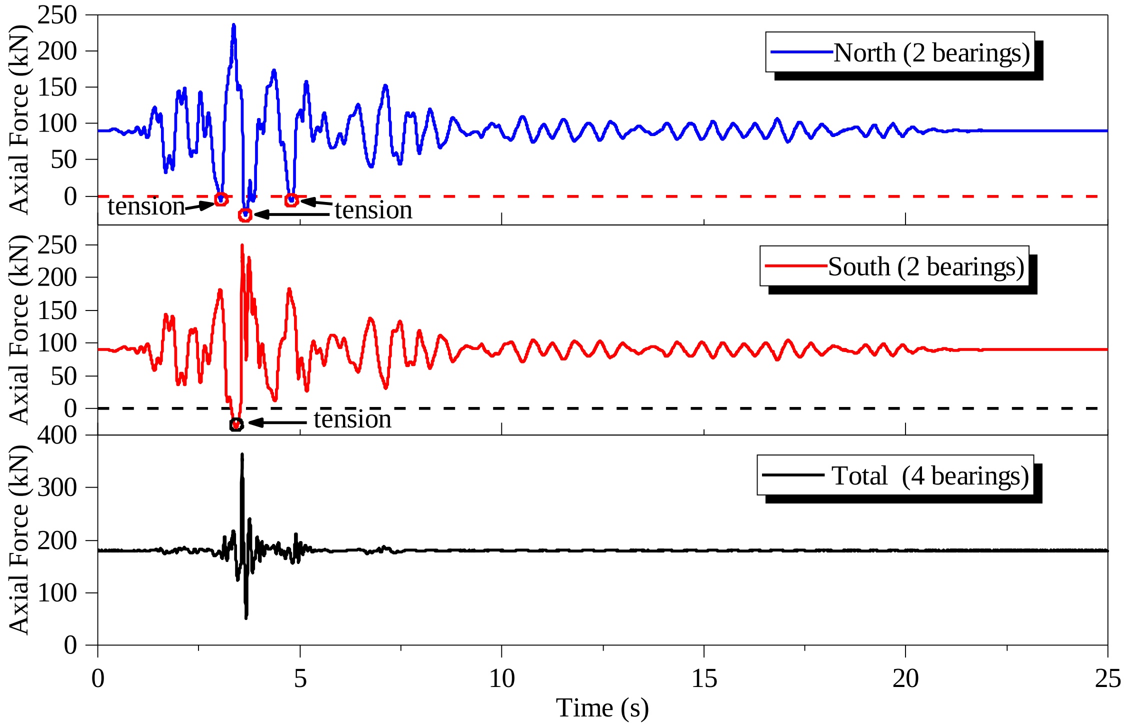

(**b**)

Figure 11. History of the record axial force of the LNRs subjected to: (**a**) ChiChi_NP_0.80 g; (**b**) Kobe_NP_0.80 g.

As shown in Figure 10b, the two south low damping rubber bearings experienced slight tension (a value less than zero) under Kobe_NP_0.60 g. In Figure 11, all four bearings experienced tension. The uplift of the entire structure affected the load cells, and the total axial force on all four bearings exhibited large variations. While for the FF ground motions, the total axial force on all four bearings exhibited little variation. The rubber bearings did not experience tension.

The maximum displacement of all four bearings under different earthquake levels are listed in Table 8. The displacements of the bearings caused by FF ground motions were smaller than those caused by NF ground motions. The Kobe_NP and ChiChi_NP ground motions caused very large displacements of the bearings. When the input PGA is 0.40 g, corresponding to the rare earthquake of intensity 8, the maximum displacement of the isolation bearing is 51.0 mm, which is smaller than the design displacement of 80 mm. When the input PGA is 0.60 g, corresponding to the extremely rare earthquake of intensity 8, the maximum displacement of the isolation bearing is 83.61 mm, which exceeds the design displacement of 80 mm. The displacement of all four bearings slightly exceeded the design displacement of 80 mm under Kobe_NP ground motion excitation with an input PGA of 0.6 g, and the displacement exceeded 100 mm when PGA was increased to 0.8 g. The time history of the northeast bearing under the Kobe_NP and ChiChi_NP ground motions are shown in Figures 12 and 13, respectively.

Table 8. Displacement of the bearings (unit: mm).

Bearings	**Ground Motion**	**PGA(g)**					
		0.1	**0.2**	**0.3**	**0.4**	**0.6**	**0.8**
Bearing northeast	Imp_F	2.0	3.2	5.4	7.2	16.3	25.7
	Kobe_F	1.7	3.0	5.4	8.0	13.8	19.8
	ChiChi_F	3.2	6.3	10.2	14.5	23.2	32.3
	Imp_N	2.0	3.4	5.4	8.3	13.4	19.0
	Kobe_NP	5.6	17.0	32.3	51.0	83.6 *	120.3 *
	ChiChi_N	3.9	9.7	13.6	19.8	39.0	56.5
	ChiChi_NP	4.4	10.8	23.4	33.0	63.3	90.5 *
Bearing southeast	Imp_F	1.8	3.6	5.5	6.9	15.6	26.2
	Kobe_F	2.3	3.7	6.0	8.0	14.2	19.3
	ChiChi_F	3.6	6.0	10.9	14.1	24.3	33.6
	Imp_N	2.1	4.2	5.8	7.4	14.2	19.1
	Kobe_NP	6.3	16.6	32.3	51.7	82.7 *	118.8 *
	ChiChi_N	4.7	9.9	13.3	20.2	38.9	57.0
	ChiChi_NP	5.3	12.1	24.0	33.0	64.4	90.4 *
Bearing northwest	Imp_F	3.2	4.1	6.7	7.8	15.8	34.0
	Kobe_F	2.4	3.7	7.1	7.6	14.2	25.6
	ChiChi_F	4.4	6.8	11.9	14.7	23.1	33.3
	Imp_N	2.5	3.7	6.3	8.1	14.4	24.0
	Kobe_NP	5.4	15.2	30.4	50.2	82.4 *	104.8 *
	ChiChi_N	3.1	8.0	13.1	18.3	37.4	60.0
	ChiChi_NP	3.9	13.0	26.0	30.8	65.7	98.4 *
Bearing southwest	Imp_F	1.9	3.2	5.1	7.1	15.3	24.7
	Kobe_F	1.7	3.0	5.6	8.2	14.8	21.2
	ChiChi_F	3.1	6.3	10.8	14.7	22.5	31.7
	Imp_N	2.1	3.8	5.8	8.3	14.5	20.5
	Kobe_NP	5.7	16.6	32.0	51.7	82.4 *	-
	ChiChi_N	4.3	9.2	13.6	20.6	39.1	55.7
	ChiChi_NP	3.5	11.4	24.9	32.7	63.6	90.9 *

* denotes that the displacement of the bearing exceeds the design displacement, and—denotes unrecorded displacement.

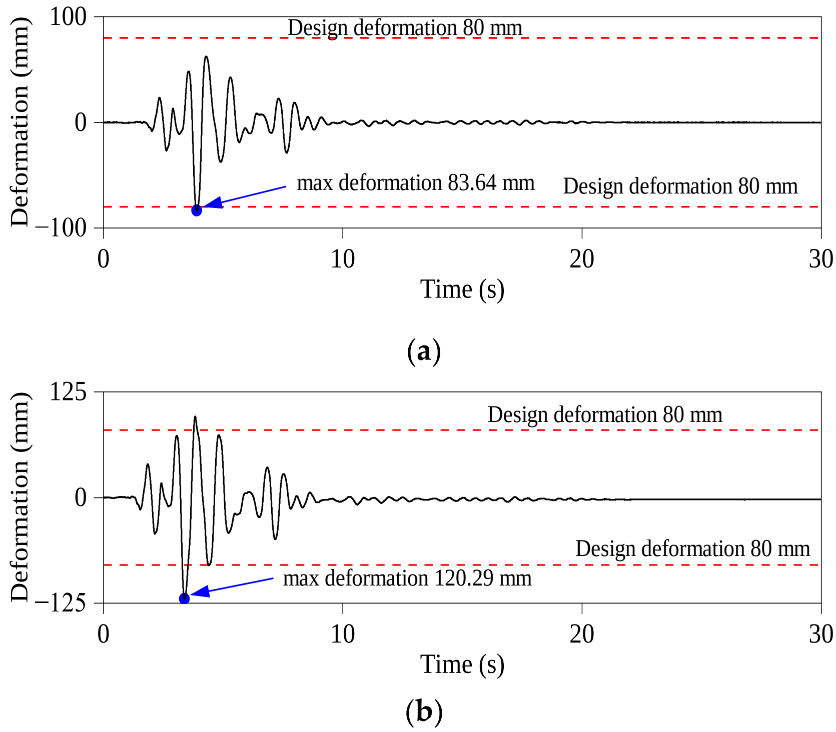

Figure 12. History of the displacement of the LNR subjected to: (**a**) Kobe_NP_0.60 g; (**b**) Kobe_NP_0.80 g.

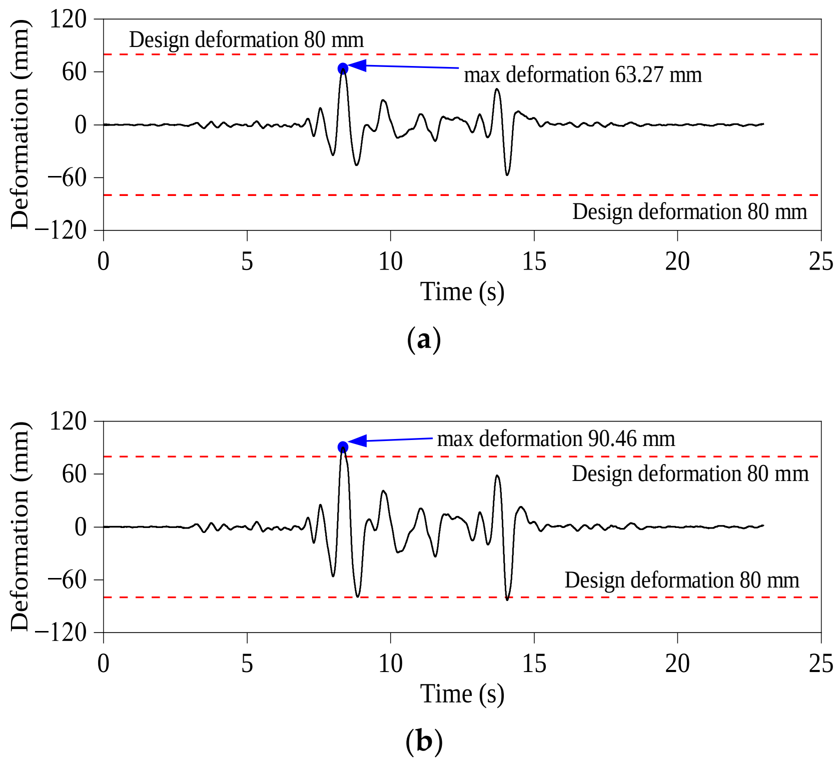

Figure 13. History of displacement of the LNR subjected to: (**a**) Kobe_NP_0.60 g; (**b**) Kobe_NP_0.80 g.

Figure 14 displays the maximum displacements of the viscous dampers subjected to excitations with different earthquake levels. The displacement response of the four viscous dampers affords similar distributions under different earthquake levels. Moreover, displacements caused by NF ground motions were significantly larger than those caused by

FF ground motions, except for the Imp_N ground motion. The response spectrum shows that in the neighborhood of the fundamental period of the isolated structure, the response spectrum value of the Imp_N ground motion is smaller than that of other NF ground motions and is close to that of FF ground motions. The damper displacement exceeds the design displacement of the damper (75 mm) under Kobe_NP ground motion with a PGA of 0.8 g. The displacement of the dampers increased with the PGA value of the excitation, and the growth rate of the displacement increased with the input PGA.

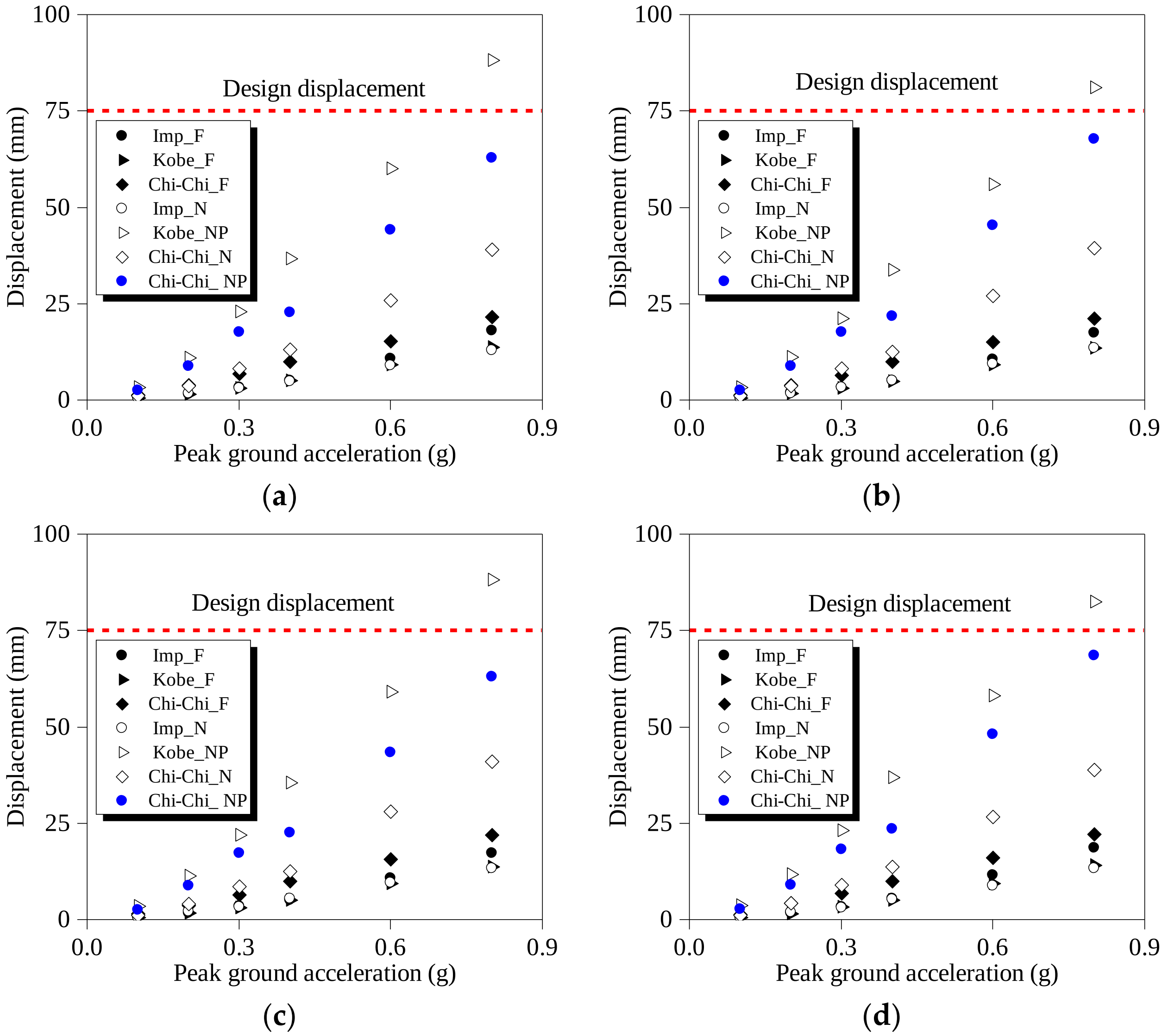

Figure 14. Maximum damper displacement in different earthquake levels: (**a**) northeast location; (**b**) southeast location; (**c**) northwest location; (**d**) southwest location.

Figure 15 displays the residual displacement of the viscous dampers. The maximum value of the residual displacement of the NLVDs was smaller than 0.5 mm until the input PGA exceeded 0.4 g. For the two dampers located in the northeast and southeast, maximum residual displacement was induced when the isolated structure was subjected to Kobe_NP_0.80 g. For the two dampers located in the northwest and southwest, maximum residual displacement was induced when the isolated structure was subjected to ChiChi_F_0.80 g. Residual displacements of the NLVDs were very small during earthquakes.

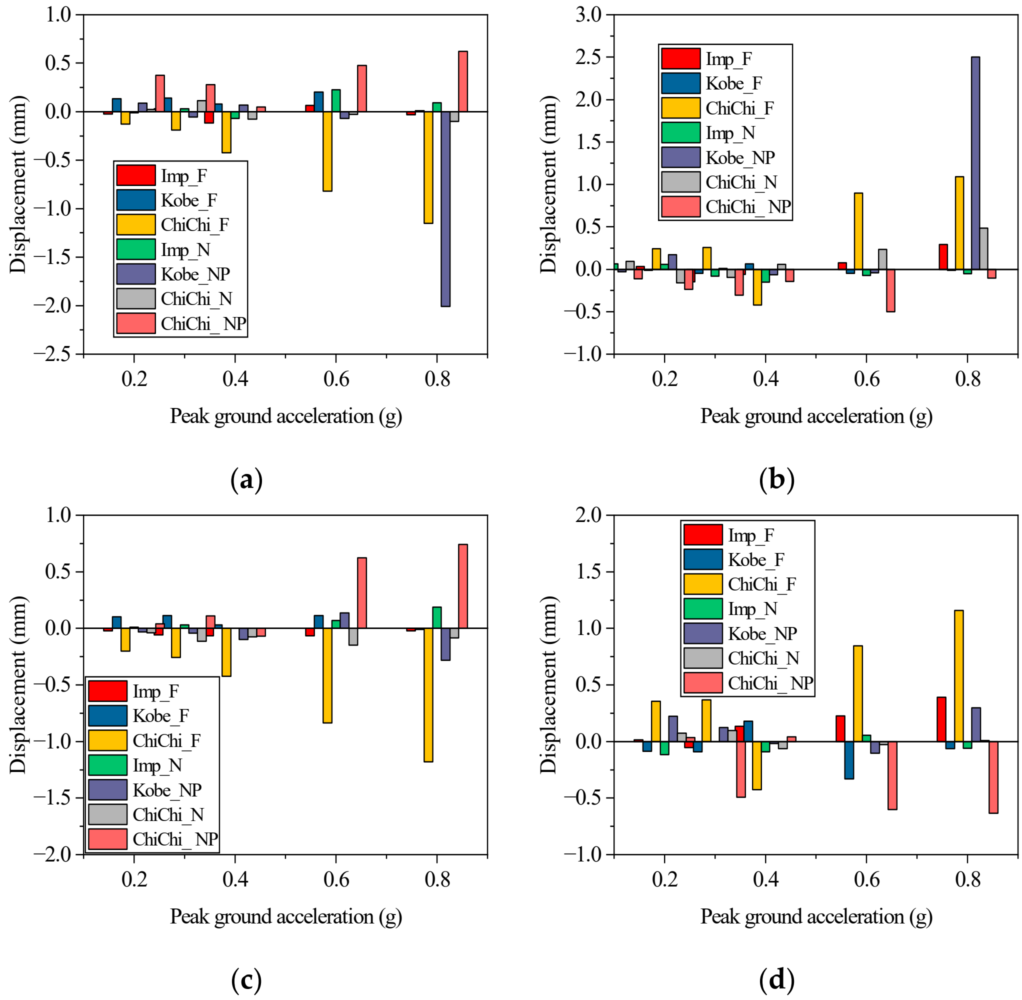

Figure 15. Residual displacement of the viscous dampers: (**a**) Northeast location; (**b**) Southeast location; (**c**) Northwest location; (**d**) Southwest location.

Peak values of the axial forces of the viscous damper are listed in Table 9. The maximum damper force occurred in the damper located in the northeast when the isolated structure was subjected to Kobe_NP_080 g. The maximum damper force was 25.46 kN, which is smaller than the design maximum damper force of 30 kN. Figure 16 displays the hysteretic curves of the four NLVDs under Kobe_NP ground motion with the input PGA of 0.80 g. The shape of the hysteretic curve is full, and it indicates that the NLVDs have a good energy dissipation effect.

Table 9. Maximum axial force of the NLVDs (unit: kN).

NLVD Location	PGA (g)					
	0.10	**0.20**	**0.30**	**0.40**	**0.60**	**0.80**
northeast	7.54	11.34	14.31	16.62	20.32	25.46
southeast	7.13	10.92	13.64	16.08	19.50	23.88
northwest	7.61	11.13	13.70	16.14	20.07	23.35
southwest	7.71	11.69	14.45	16.74	20.18	24.56

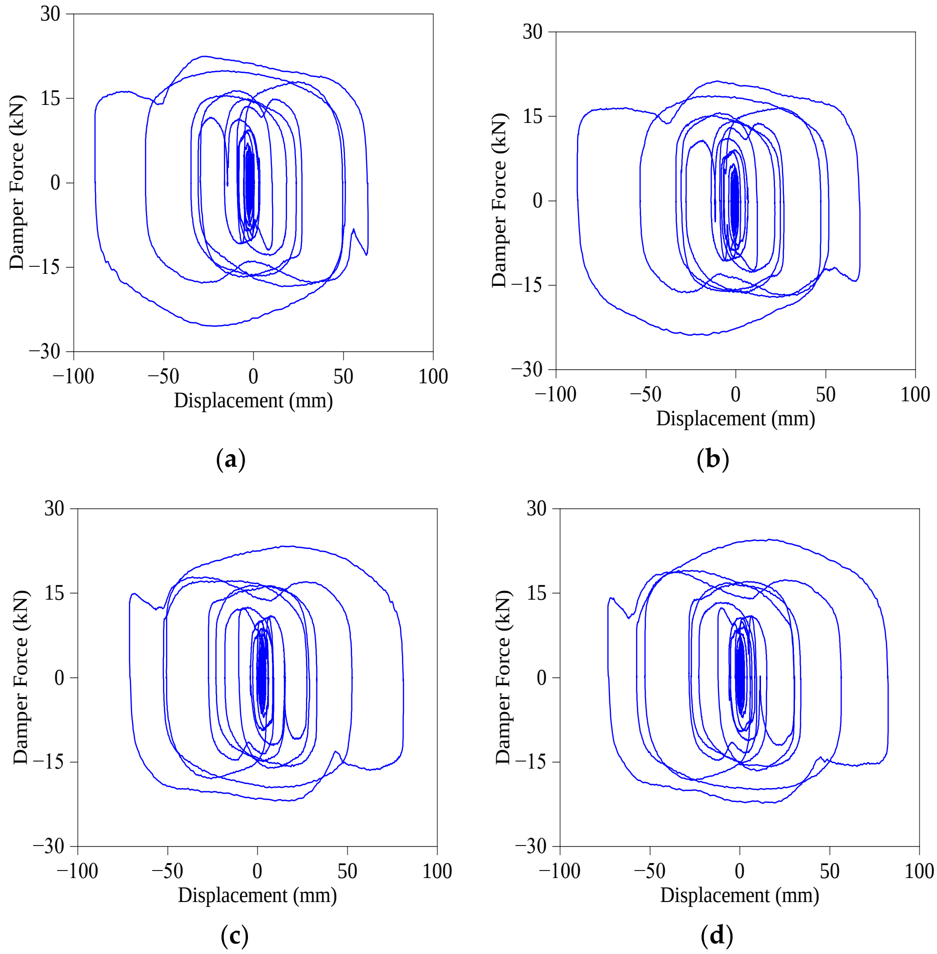

Figure 16. Hysteretic curve of the viscous dampers under Kobe_NP ground motion with a PGA of 0.80 g: (**a**) Northeast location; (**b**) Southeast location; (**c**) Northwest location; (**d**) Southwest location.

5. Conclusions

The shaking table test was conducted for a five-story building model in the moment frame in conjunction with isolation systems. The isolation systems utilized were LNRs with additional NLVDs. Seven ground motions, including three FF ground motions and four NF ground motions, were employed for the shaking table test. Compared with the existing studies, the novelty of the current study is that it experimentally investigates the seismic performance of isolation systems with passive control devices and superstructures subjected to NF ground motions. The main conclusions of the paper are as follows:

1. NF ground motions caused larger inter-story drifts than FF ground motions, especially when the input PGA exceeded 0.4 g. The Kobe_NP NF ground motion with pulse period T_p neighboring the fundamental period of the isolated structure caused the largest inter-story drift and floor acceleration of the superstructure.
2. NF ground motions cause larger base shear force of the isolation system compared with FF ground motions. Pulse-like NF ground motions, e.g., Kobe_NP and ChiChi_NP ground motions, caused a considerably large base shear for the isolation system. The base shear exceeded the total weight of the isolated structure. The axial load of the isolation bearings experienced tension under the pulse-like NF ground motion excitations because of a large overturning moment. The large overturning moment caused an uplift of the LNR when the isolated system was subjected to pulse-like NF ground motions with a large PGA value.
3. The displacements of the LNRs caused by FF ground motions were smaller than those caused by NF ground motions. The displacement of all four bearings slightly

exceeded the design displacement of 80 mm under Kobe_NP pulse-like NF ground motion excitation with a PGA of 0.6 g, and the displacement exceeded 100 mm when the PGA was increased to 0.8 g.

4. Nonlinear viscous dampers performed well during the earthquake simulations; the maximum displacement and damper force were within the design value. The residual displacements of the viscous dampers were very small under NF ground motions. NLVDs protected the LNRs very under NF ground motions, but the severe responses of the LNRs could be caused by NF ground motion with pulse period T_p neighboring the fundamental period of the isolated structure.

In this paper, the seismic performance of base-isolated structures with viscous dampers was studied, and the performance of isolation bearing and viscous damper was also evaluated. Although viscous dampers have performed well in reducing isolation structure under near-field earthquakes, the large deformation of the isolation layer was caused for near-field earthquakes with the pulse period neighboring the period of the isolated structure. The combination of dampers with different mechanisms or new dampers should be further used to control the deformation of the isolation layer under large near-field earthquakes without affecting the isolation effect under moderate earthquakes. The corresponding calculation analysis and experimental study should be carried out in the future.

Author Contributions: Conceptualization, Q.L. and B.F.; methodology, Q.L. and W.L.; validation, B.F. and L.L.; formal analysis, Q.L.; investigation, Q.L.; resources, W.Q. and M.Z.; data curation, Q.L. and Z.Z.; writing—original draft preparation, Q.L.; writing—review and editing, B.F. and B.Z.; visualization, W.Q. All authors have read and agreed to the published version of the manuscript.

Funding: This study was supported by the National Natural Science Foundation of China (Grant Nos. 52008216, 51908129, 51908048); the Opening Funds of State Key Laboratory of Building Safety and Built Environment and National Engineering Research Center of Building Technology (Grant No. BSBE2019-01); the Scientific Research Fund of Institute of Engineering Mechanics, China Earthquake Administration (Grant No. 2020D22); the Basic Public Welfare Research Project of Zhejiang Province, China (Grant No. LGG21E080007); and the Natural Science Foundation of Zhejiang province, China (Grant No. LY20A020005).

Data Availability Statement: Some or all data that support the findings of this study are available from the corresponding author upon reasonable request.

Acknowledgments: Thanks are due to Kaiqi Yu for assistance with the experiments and to Dayang Wu and Peng Zhang for valuable discussion.

Conflicts of Interest: The authors declare no conflict of interest.

References

1. Rong, Q. Optimum parameters of a five-story building supported by lead-rubber bearings under near-fault ground motions. *J. Low Freq. Noise, Vib. Act. Control* **2020**, *39*, 98–113. [CrossRef]
2. Bhandari, M.; Bharti, S.D.; Shrimali, M.K.; Datta, T.K. Seismic Fragility Analysis of Base-Isolated Building Frames Excited by Near- and Far-Field Earthquakes. *J. Perform. Constr. Facil.* **2019**, *33*, 1–16. [CrossRef]
3. Hall, J.F.; Heaton, T.H.; Halling, M.W.; Wald, D. Near-Source Ground Motion and its Effects on Flexible Buildings. *Earthq. Spectra* **1995**, *11*, 569–605. [CrossRef]
4. Jangid, R.S.; Kelly, J.M. Base isolation for near-fault motions. *Earthq. Eng. Struct. Dyn.* **2001**, *30*, 691–707. [CrossRef]
5. Jangid, R. Optimum lead–rubber isolation bearings for near-fault motions. *Eng. Struct.* **2007**, *29*, 2503–2513. [CrossRef]
6. Providakis, C. Pushover analysis of base-isolated steel–concrete composite structures under near-fault excitations. *Soil Dyn. Earthq. Eng.* **2008**, *28*, 293–304. [CrossRef]
7. Mazza, F.; Vulcano, A. Nonlinear response of RC framed buildings with isolation and supplemental damping at the base subjected to near- fault earthquakes. *J. Earthq. Eng.* **2009**, *13*, 690–715. [CrossRef]
8. Bhagat, S.; Wijeyewickrema, A.C. Seismic response evaluation of base-isolated reinforced concrete buildings under bidirectional excitation. *Earthq. Eng. Eng. Vib.* **2017**, *16*, 365–382. [CrossRef]
9. Bhagat, S.; Wijeyewickrema, A.C. Seismic collapse probability considering pounding and financial loss estimation of base isolated reinforced concrete buildings. *J. Earthq. Tsunami* **2018**, *12*, 1–21. [CrossRef]
10. Nagarajaiah, S.; Ferrell, K. Stability of elastomeric seismic isolation bearings. *J. Struct. Eng.* **1999**, *125*, 946–954. [CrossRef]

11. Vestroni, F.; Vulcano, A.; Di Pasquale, G. Earthquake response analysis of a nonlinear model of a base-isolated structure. In Proceedings of the International Meeting on Earthquake Protection of Buildings, Ancona, Italy, 6–8 June 1991.
12. Mazza, F.; Vulcano, A. Seismic response of buildings with isolation & supplemental dissipation at the base. In Proceedings of the 5th World Congress on Joints, Bearings and Seismic Systems for Concrete Structures, Rome, Italy, 7–11 October 2001.
13. Kelly, J.M. The role of damping in seismic isolation. *Earthq. Eng. Struct. Dyn.* **1999**, *28*, 3–20. [CrossRef]
14. Ahmet, H.D.; Huseyin, B. Effects of the isolation parameters on the seismic response of steel frames. *Earthq. Struct.* **2018**, *15*, 319–334.
15. Kun, Y.; Yan, X.; Liang, H. A direct displacement-based design procedure for base-isolated building structures with lead rubber bearings (LRBs). *Eng. Struct.* **2019**, *197*, 1–9.
16. Ayoub, S.; Gholamreza, G.A.; Mohammad, S. Effects of ductility and connection design on seismic responses of base-isolated steel moment-resisting frames. *Soil Dyn. Earthq. Eng.* **2021**, *143*, 1–19.
17. Alataby, E.K.; Kadhim, J.A.; Ahmed, M.A. Study on the Effect of Distribution of Viscous Damper for Steel Frame Structure. *J. Phys. Conf. Ser.* **2021**, *1973*, 012220. [CrossRef]
18. Makris, N.; Chang, S.P. Effect of viscous, viscoplastic and friction damping on the response of seismic isolated structures. *Earthq. Eng. Struct. Dyn.* **2000**, *29*, 85–107. [CrossRef]
19. Palazzo, B.; Petti, L. Combined control strategy: Base isolation and tuned mass damping. *ISET J. Earthq. Technol.* **1999**, *36*, 121–137.
20. Zhang, Y.; Iwan, W.D. Protecting base isolated structures from near-field ground motion by tuned interaction damper. *J. Eng. Mech.* **2002**, *128*, 287–295. [CrossRef]